JOURNAL OF APPLIED ELECTROCHEMISTRY 19 (1989) 1–9

A high performance molten carbonate fuel cell cathode

MARK FRANKE, JACK WINNICK

School of Chemical Engineering, Georgia Institute of Technology, Atlanta, GA 30332-0100, USA

Received 22 March 1988; revised 2 July 1988

A highly-conducting ceramic material, identified as stable in molten carbonate electrolyte, has been fabricated by partial sintering of the powder into porous gas-diffusion electrodes. These have been tested with commercial molten carbonate electrolyte 'tiles', to compare performance with that of state-of-the-art NiO cathodes. Although the fabrication technique was quite simple, the resultant $La_{0.8}Sr_{0.2}CoO_3$ electrodes showed kinetic performance equivalent to the NiO. This, or other perovskite or spinel-structure ceramic shown to be totally system compatible in long-term tests, can be formed into effective electrodes to replace NiO.

1. Introduction

The molten carbonate fuel cell (MCFC) is directed at large-scale power generation which can utilize a wide variety of fossil fuels at very high efficiency and with minimal pollution. In order for the MCFC to compete with traditional power sources on an economic basis, the operational lifetime of a commercial unit is required to approach 40 000 h [1, 2]. In order to achieve such a life several problems must be overcome, including electrode dissolution [3, 4], pore structure degradation [5] and electrolyte losses due to corrosion [6], evaporation [7, 8] and migration [9]. While the anode seems to be near design goals, the cathode continues to be problematical.

The standard MCFC cathode is NiO, formed from porous Ni plaques, oxidized *in situ*. Recent studies have shown NiO is slightly soluble in the molten carbonate electrolyte [3, 4]; the solubility has been found to be a function of the acid/base chemistry of the melt [10]. In an operating cell, an effective oxygen concentration gradient is set up within the electrolyte membrane [4, 11], continuously decreasing from the cathode interface to the anode interface. As the dissolved NiO diffuses through the membrane a point is reached where the local oxygen concentration drops below the NiO stability limit. At this point metallic nickel precipitates, forming nickel 'sinks' within the electrolyte membrane. This process degrades both the cathode and membrane structures, and results in decreasing cell performance or even failure. These considerations have stimulated a search for alternative cathode materials which overcome these problems.

Baumgartner *et al.* [11] surveyed a variety of mixed metal oxides as candidate materials for the MCFC cathode. They evaluated the materials on the basis of electronic conductivity and stability in the molten carbonate electrolyte. Only two of the tested materials satisfied both criteria: $La_xSr_{1-x}CoO_3$ and $LaNiO_3$. Of these, the $La_xSr_{1-x}CoO_3$ displayed the higher conductivities, approximately 35 $(ohm\,cm)^{-1}$ for $x = 0.6$ and 20 $(ohm\,cm)^{-1}$ for $x = 0.8$. A more comprehensive long-term stability study [12] indicated that the lanthanum oxides were slightly reactive with the $LiAlO_2$ matrix of the electrolytic membrane, for example

$$LaCoO_3 + LiAlO_2 \longrightarrow LaAlO_3 + LiCoO_2 \quad (1)$$

This result indicates that an alternative matrix material, which alleviates the stability problem, would have to be identified in order to use the lanthanum oxides as the cathode material in long-term applications. The same study [12] identified $SrTiO_3$ as such a material, overcoming these stability problems.

A successful cathode must, in addition to satisfying the above material criteria, be able to be formed into an efficient gas-diffusion electrode. That is, a procedure must be developed to form a mechanically sound structure with large gas pores and a fine-pore pattern sufficient to create electrolyte-wetted pore boundaries. The capillary forces set up in the electrode must not be so great as to flood the large gas pores; the capillary in the electrolyte membrane (or 'tile') must not be overcome. The high conductivity of $La_xSr_{1-x}CoO_3$ coupled with its compatibility with the carbonate made it a reasonable choice for a test of electrode fabrication and performance. The first step was to develop a technique which would allow the perovskite material to be processed into an efficient electrode structure. The next phase of research, and the one focused on in this paper, was to evaluate the performance of the perovskite electrodes in a bench-scale MCFC. In preliminary experiments, the perovskite electrodes exhibited performance comparable to that of commercial NiO electrodes [13]. However, the perovskite electrodes utilized in these tests had a pore and particle size roughly an order of magnitude larger than NiO electrodes. It was expected that a finer structure would enhance the active area and result in improved polarization behavior. Here, we report a more comprehensive performance study of the finer structure perovskite electrodes.

2. Experimental details

The $La_{0.8}Sr_{0.2}CoO_3$ perovskite material was prepared by ball-milling stoichiometric quantities of the corresponding metal acetates to a homogeneous powder

0021-891X/89 $03.00 + .12 © 1989 Chapman and Hall Ltd.

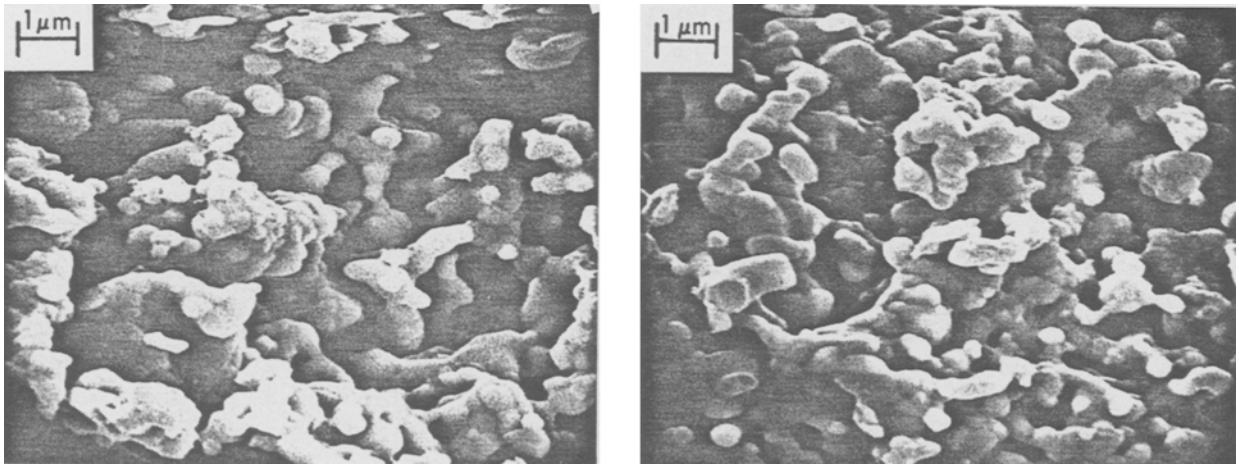

Fig. 1. Scanning electron micrographs of: (a) a perovskite electrode; and (b) a Ni electrode, furnished by Gould and oxidized *in situ*.

(> 6 h) and then decomposing the powder in air for 1 h at each of the consecutive temperatures: 150, 200, 250, 300 and 500° C. The resultant perovskite material was then ground and sieved to the smallest particle size (sub-38 micron). The electrodes were fabricated by pressing the perovskite powder in a die at 25 kg cm^{-2} pressure and then sintering in air at 1100° C overnight. This procedure resulted in an electrode disc approximately 1.0 mm thick with a porosity of 65% and a conductivity of 0.3 (ohm cm)$^{-1}$ (600° C). Figure 1 displays an electron micrograph of a perovskite electrode and, for comparison, an electron micrograph of a NiO electrode (Ni, supplied by Gould Inc., oxidized *in situ*). A BET surface area analysis indicated 0.5 m^2 g^{-1} for both materials. These indicate that the two materials are of similar particle and pore sizes.

A diagram of the test cell is shown in Fig. 2. The cell housings were made of Macor, a machinable glass ceramic. The Macor material appeared to be completely inert to the carbonate electrolyte, at least for the relatively short duration runs of this investigation (200 h). Each housing provided inlet and outlet gas ports and a baffled gas flow channel adjacent to the porous electrodes. The baffles were gold plated and act as both an electrode support and a current distributor. The housings were machined to accommodate an electrode disc 1.0 mm thick, with a geometric area of 7.92 cm^2. Electrical connections to the electrodes were made with gold wires fed into the cell through the gas outlet ports. The top housing provided an extra machined port for a reference electrode. The reference electrode was a gold wire bathed in 30% CO_2, 70% air. Cell potentials and currents were controlled

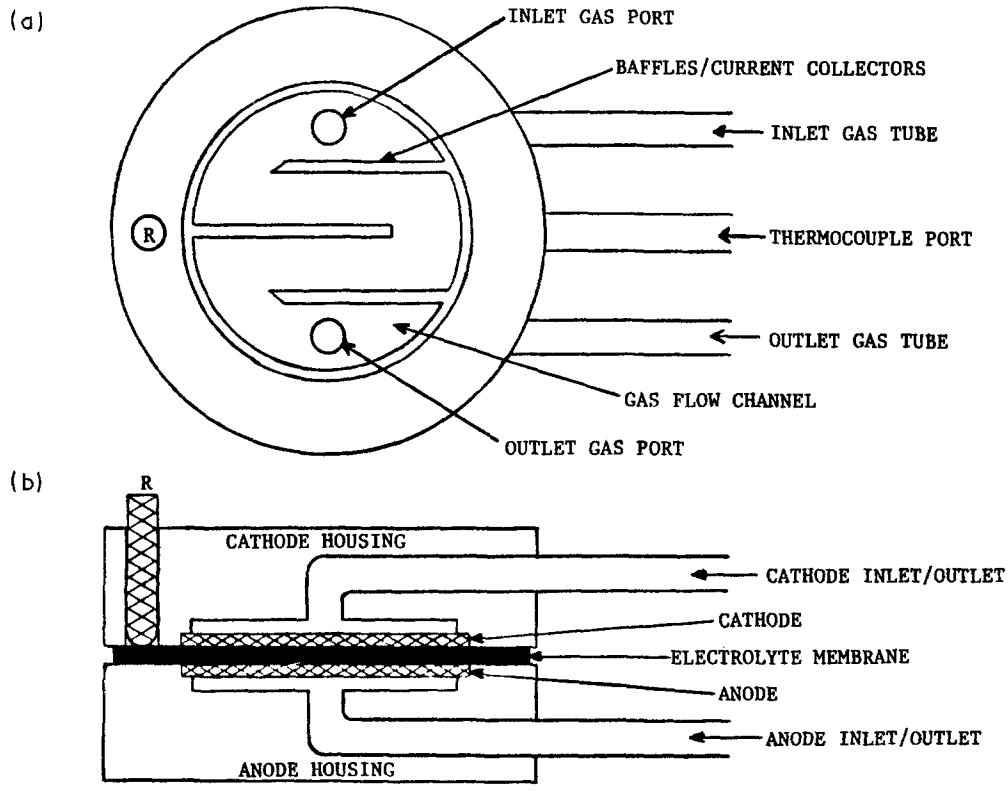

Fig. 2. Schematic of membrane cell: (A) cell housing; (B) assembled cell cross-section.

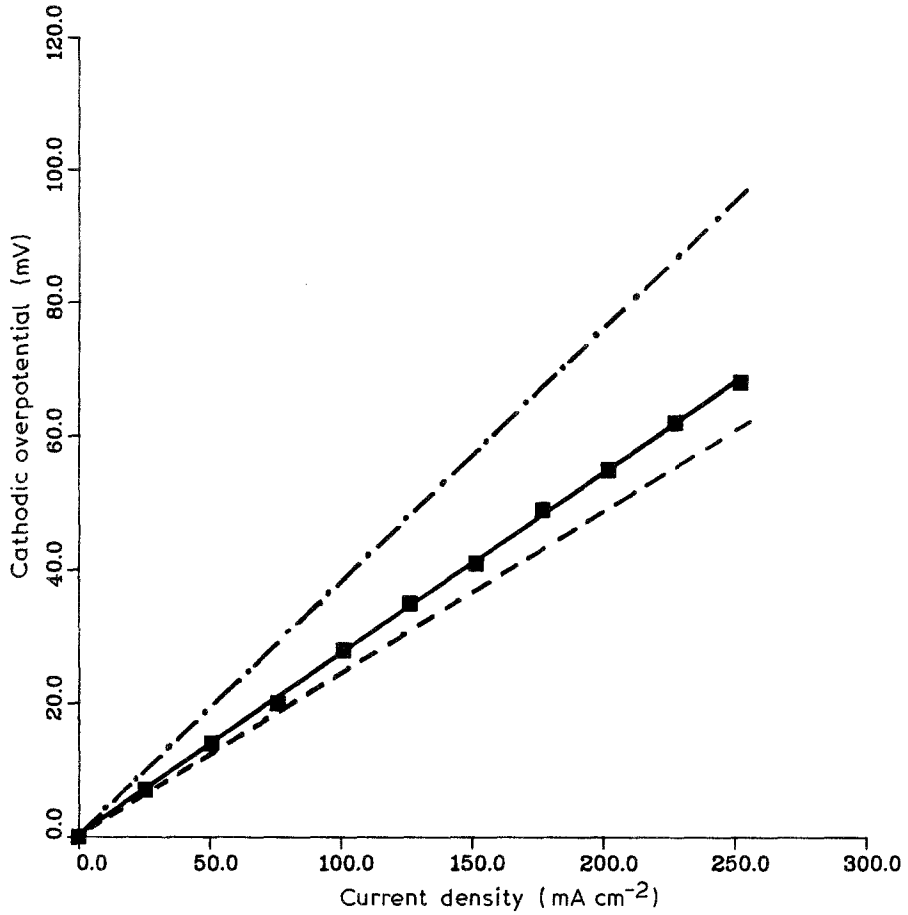

Fig. 3. *IR*-free cathodic polarizations at 650° C, under standard oxidant conditions (15% O_2, 30% CO_2 in N_2). (■—■—■) perovskite; (– – – –) NiO [14]; (–·–·–) NiO [15].

with a PAR-371 Potentiostat/Galvanostat with a model 178 electrometer probe. Cell potentials were monitored with Simpson Model 460 digital multimeters (± 0.1 mV accuracy); a Tektronix model 5111 storage oscilloscope was utilized to measure the cell ohmic resistance via the current interruption method.

Perovskite electrodes were used as both cathode and anode in the MCFC. The oxidant gas, mixed from individual standard grade CO_2, O_2 and N_2 gas cylinders with Matheson model 600, 601 and 602 rotameters, was fed into both cathode and anode compartments. The range of partial pressures investigated was 0.5–50.0% for both CO_2 and O_2. The total flow rate to the cathode compartment was always 400 $cm^3 min^{-1}$ except at low partial pressure of either active component (0.5% or 2.0%) where the flow rate was 1000 $cm^3 min^{-1}$. Utilization was always less than 80% and was typically below 20%. At the higher utilizations, checks were made to assure flow rate had no effect on the polarization performance. The temperature range investigated was 550–650° C. Care was taken to ensure that potentials were not recorded before the cell had reached steady state.

3. Results

IR-free polarizations of the perovskite cathode under standard MCFC oxidant conditions are displayed in Fig. 3. In addition, the figure shows *IR*-free polarizations of NiO cathodes reported by the Institute of Gas Technology (IGT) under otherwise identical conditions [14, 15]. The data show the polarization behavior of the perovskite is comparable to that of the NiO. The perovskite data in the low polarization region were used to estimate the exchange current density, i_0 (superficial area basis).

$$i_0 = \frac{di}{d\eta}\left(\frac{RT}{2F}\right) \tag{2}$$

where i is the current density and η is the cathodic overpotential. Linear regression produced an i_0 value of 148 mA cm^{-2}. This value is consistent with the NiO data in Fig. 3, where the i_0 values were 154 mA cm^{-2} (estimated from [14]) and 134 mA cm^{-2} (reported in [15]). However, a direct quantitative comparison may involve some error since the MCFC set-up used in our laboratory is not identical to that used by IGT.

Figure 4 displays additional data comparing the cathodic polarization behavior of the two electrode materials. A direct comparison can be made with greater confidence in this case since the two MCFC set-ups are virtually identical. The data show the performance of the perovskite cathode is comparable and actually slightly better than the NiO. The exchange current densities derived from the data in Fig. 4 are reported in Table 1, extrapolated from high polarization data. The perovskite values are seen to be approximately 10% higher than the NiO.

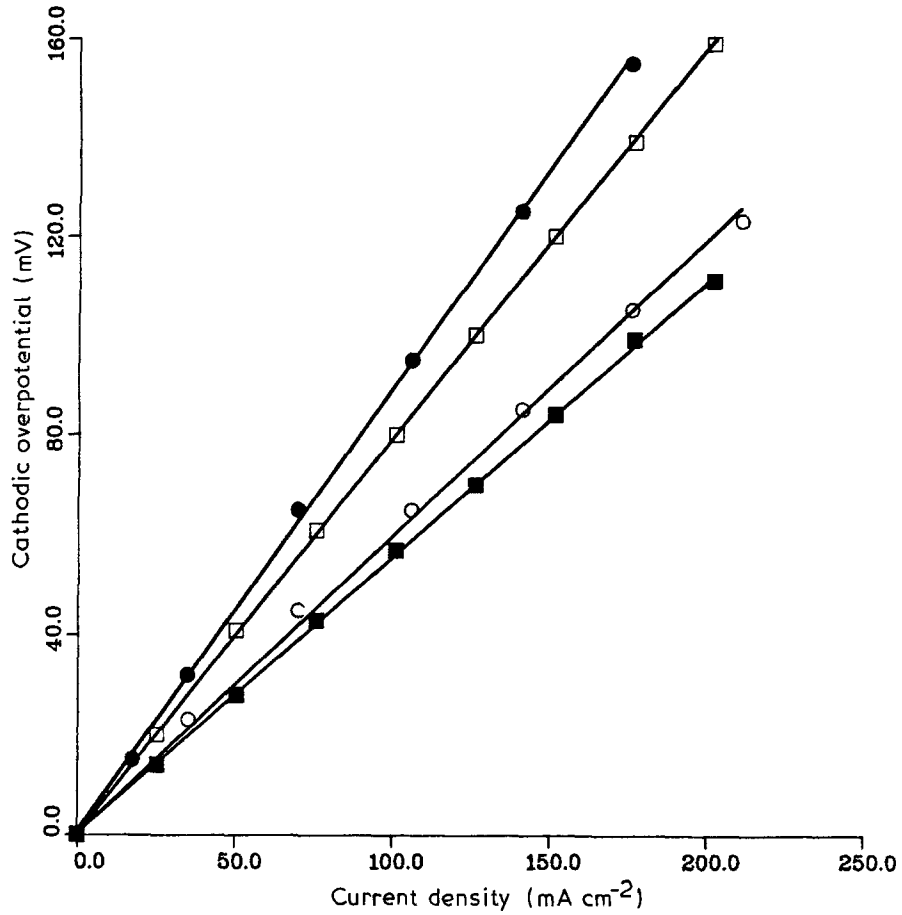

Fig. 4. *IR*-free cathodic polarizations at 590° C. ■ = perovskite, 19% O_2, 50% CO_2; □ = perovskite, 19% O_2, 10% CO_2; ○ = NiO [16], 19% O_2, 50% CO_2; ● = NiO [16], 19% O_2, 10% CO_2.

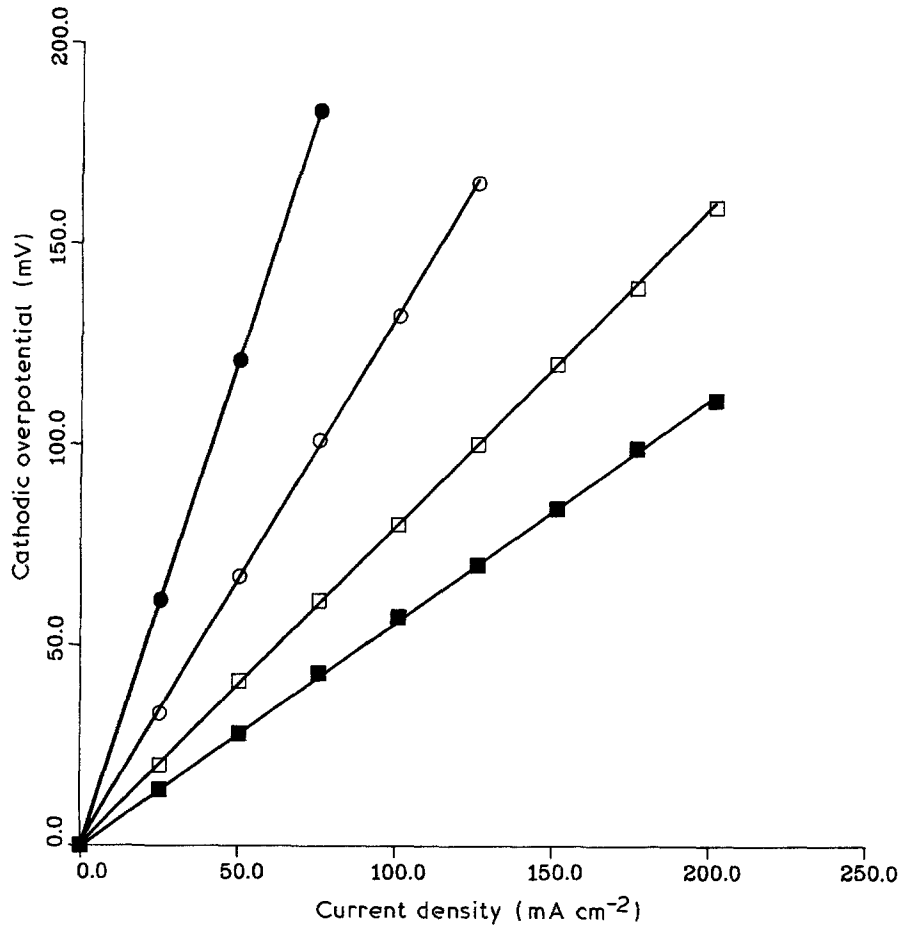

Fig. 5. *IR*-free cathodic polarizations of perovskite at 590° C with varying carbon dioxide partial pressure. ■ = 50% CO_2, 20% O_2 in N_2; □ = 10% CO_2, 20% O_2 in N_2; ○ = 2.0% CO_2, 20% O_2 in N_2; ● = 0.5% CO_2, 20% O_2 in N_2.

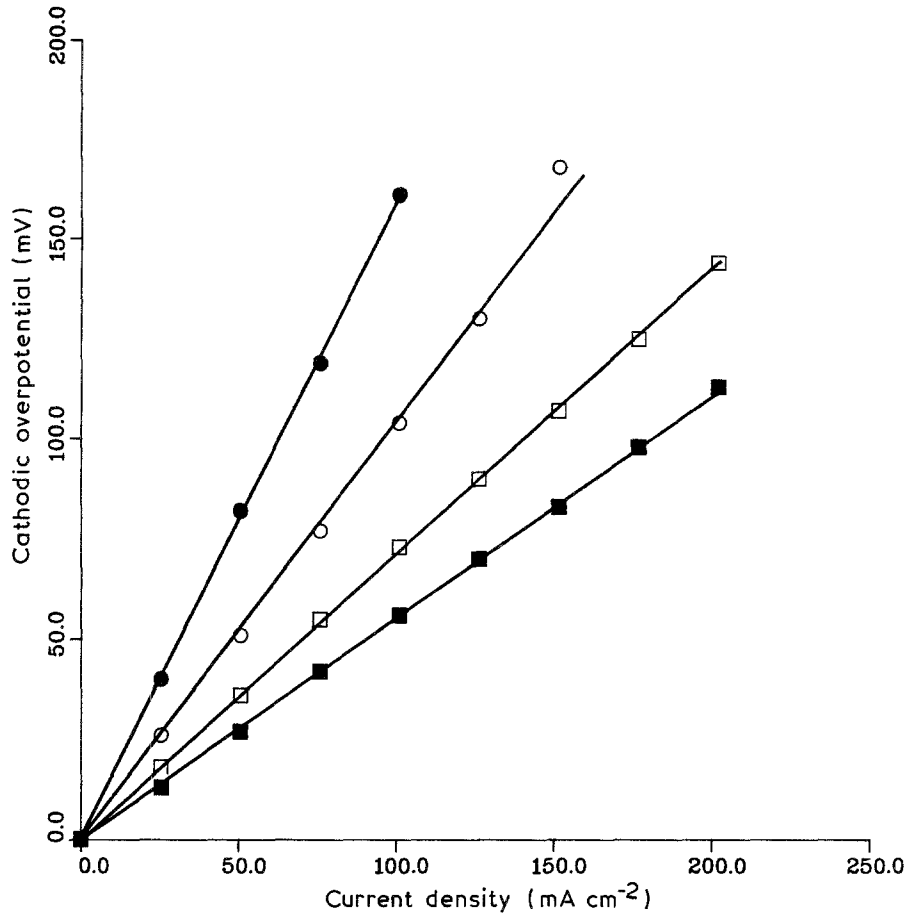

Fig. 6. *IR*-free cathodic polarizations of perovskite at 590° C with varying oxygen partial pressure. ■ = 50% O_2, 20% CO_2 in N_2; □ = 10% O_2, 20% CO_2 in N_2; ○ = 2.0% O_2, 20% CO_2 in N_2; ● = 0.5% O_2, 20% CO_2 in N_2.

In order to characterize the cathode process, the effect of partial pressures and temperature were examined. Figures 5 and 6 show the influence on polarization behavior. It is clear that both gaseous reactants have a fairly strong effect on the performance. Similarly, Fig. 7 shows that temperature also has a strong influence on the polarization performance. The data in these figures were correlated to Equation 1 to determine the corresponding exchange current densities; Table 2 exhibits the results. Figures 8 and 9 display the quantitative relationship between the exchange current density and partial pressures, and the exchange current density and temperature, respectively. The least squares correlation which results from this analysis is

$$i_0 = 50\,000 P_{CO_2}^{0.33} P_{O_2}^{0.25} \exp\left(\frac{-11\,000}{T + 273}\right) \quad (3)$$

where i_0 is in A cm^{-2} (superficial area) for T from 550 to 650° C and partial pressures from 0.005 to 0.5 atm.

Table 1. Exchange current densities (superficial area basis) calculated from the data in Fig. 4 at 590° C

Cathode material	*Gas composition*	i_0 (*mA cm*$^{-2}$)
Perovskite	19% O_2, 50% CO_2	67
NiO	19% O_2, 50% CO_2	60
Perovskite	19% O_2, 10% CO_2	47
NiO	19% O_2, 10% CO_2	39

In a similar analysis by Winnick and Ross [16] using NiO cathodes, the correlation which resulted was

$$i_0 = 150 P_{CO_2}^{0.0} P_{O_2}^{0.5} \exp\left(\frac{-6000}{T + 273}\right) \quad (4)$$

In their work, the low polarization data with varying CO_2 partial pressure exhibited a large degree of scatter. They determined the most reasonable exponent for CO_2 to be 0.0. The two correlations are considerably different, possibly indicating the cathodic reaction mechanism with perovskite is different than with NiO.

Table 2. Summary of the exchange current densities (superficial area basis) calculated from the perovskite polarization data in Figs 5–7 at various temperatures and gas compositions

Temperature (° C)	*Gas composition*	i_0 (*mA cm*$^{-2}$)
590	20% CO_2, 50% O_2	74
590	20% CO_2, 10% O_2	52
590	20% CO_2, 2.0% O_2	36
590	20% CO_2, 0.5% O_2	24
590	50% CO_2, 20% O_2	67
590	10% CO_2, 20% O_2	47
590	2.0% CO_2, 20% O_2	28
590	0.5% CO_2, 20% O_2	16
650	30% CO_2, 15% O_2	145
600	30% CO_2, 15% O_2	81
590	30% CO_2, 15% O_2	62
550	30% CO_2, 15% O_2	35

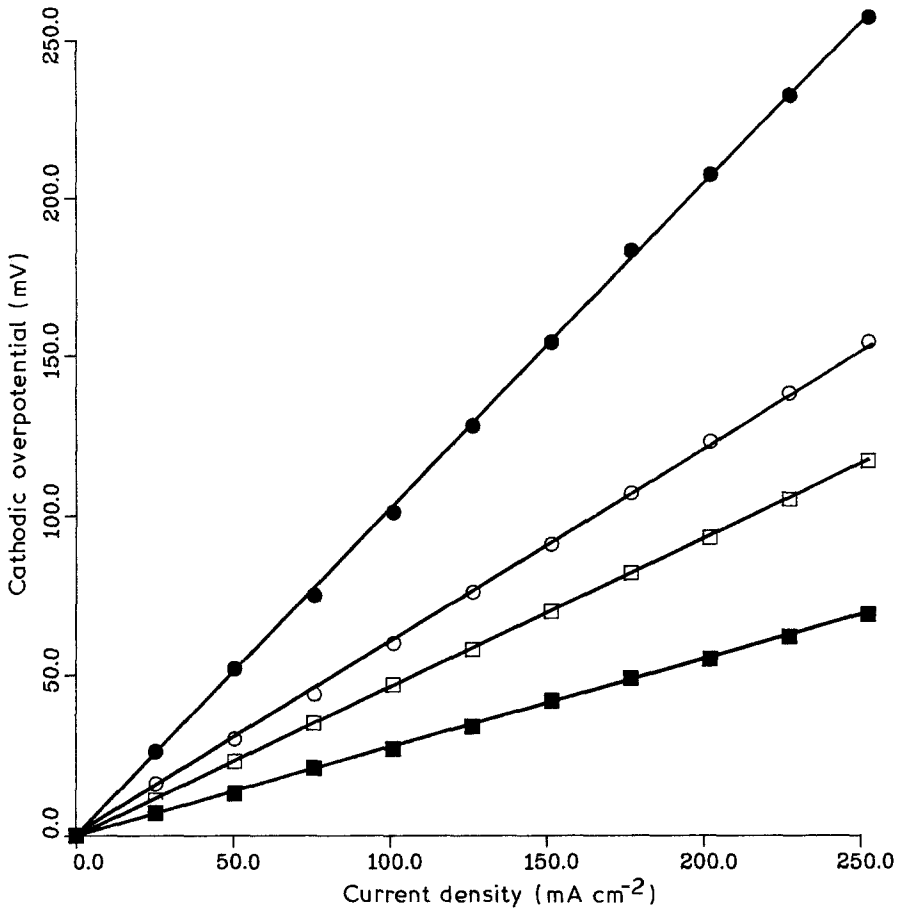

Fig. 7. *IR*-free cathodic polarizations of perovskite at varying temperature under standard oxidant conditions (15% O_2, 30% CO_2 in N_2). ■ = 650° C; □ = 600° C; ○ = 590° C; ● = 550° C.

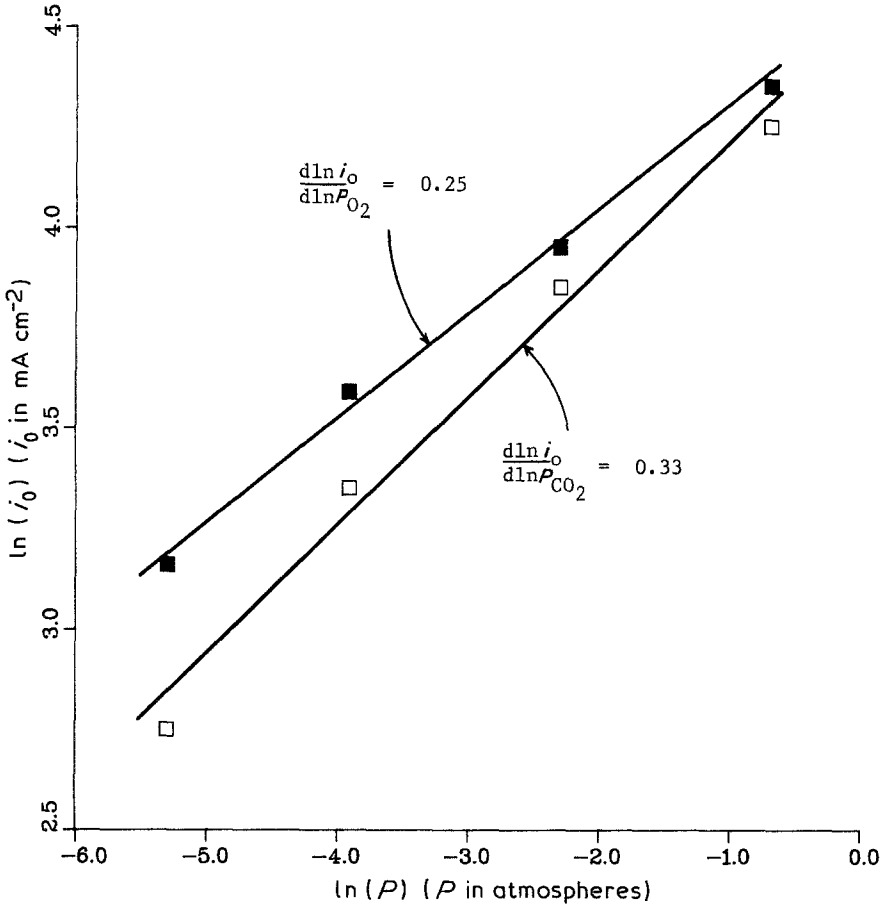

Fig. 8. Relationship between the exchange current density (on a superficial area basis) and the partial pressures of carbon dioxide and oxygen. ■ = O_2, □ = CO_2.

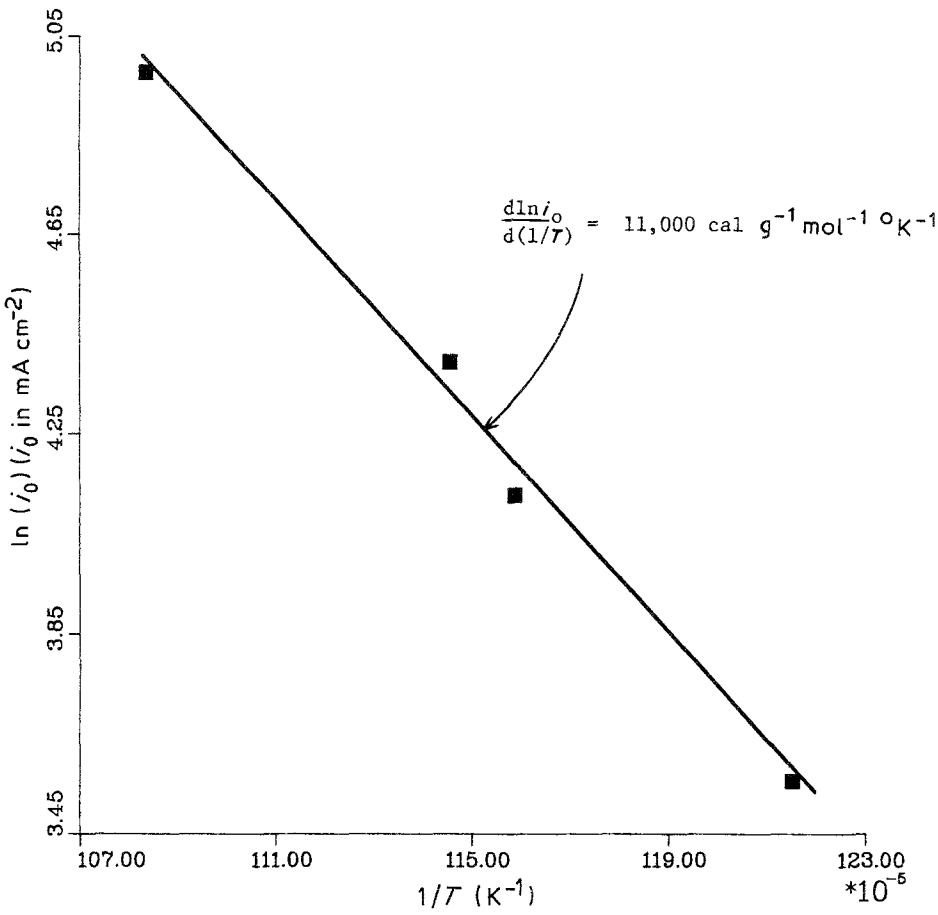

Fig. 9. Relationship between the exchange current density (on a superficial area basis) and the temperature.

More insight on the cathodic reaction mechanism can be obtained with knowledge of the transfer coefficients and reaction orders. The Butler–Volmer equation was used as a starting point

$$i = i_0[\exp(\alpha_+ \eta f) - \exp(-\alpha_- \eta f)] \quad (5)$$

where $f = F/RT$, η is the IR-free overpotential, α_+ is the anodic transfer coefficient and α_- is the cathodic transfer coefficient ($\alpha_+ + \alpha_- = 2$). For low η, Equation 4 simplifies to Equation 1. At high η,

$$i = i_0 \exp(\alpha_{+/-} \eta f) \quad (6)$$

where i and η are the absolute values of current and overpotential and $\alpha_{+/-}$ is α_+ for an anodic overpotential or α_- for a cathodic overpotential. Anodic and cathodic polarization data are plotted in Tafel form in Figs 10 and 11, respectively. The intercepts in these figures, $\eta = 0$, are the exchange current densities, calculated from data in the low polarization region. The linear portions of the Tafel plots extrapolate to the corresponding exchange current densities, indicating the polarization behavior was most likely not limited by diffusion. The slopes of the lines in these figures show $\alpha_+ = 1.15$ and $\alpha_- = 0.75$. These values are somewhat different than those found using NiO cathodes [16], where it was found that $\alpha_+ = 1.6$ and $\alpha_- = 0.5$.

The reaction orders of CO_2 and O_2 can be obtained from the partial pressure dependence of i_0 (Fig. 8) and the values of the transfer coefficients, α_+ and α_-. The anodic and cathodic reaction orders, x_a and x_c, for both CO_2 and O_2, after accounting for the Nernst effect are then [17]

$$x_{a,CO_2} = m_{CO_2} - 1 + \left(\frac{\alpha_-}{2}\right) \quad (7)$$

$$x_{c,CO_2} = m_{CO_2} + \left(\frac{\alpha_-}{2}\right) \quad (8)$$

$$x_{a,O_2} = m_{O_2} - \frac{1}{2} + \left(\frac{\alpha_-}{4}\right) \quad (9)$$

$$x_{c,O_2} = m_{O_2} + \left(\frac{\alpha_-}{4}\right) \quad (10)$$

where m_{CO_2} and m_{O_2} are the slopes, $\partial \ln i_0 / \partial \ln P$, of Fig. 8 for CO_2 and O_2, respectively. Table 3 summarizes the reaction order results for the perovskite and, in addition, lists the corresponding reaction orders derived for NiO [16]. Cathodically, CO_2 partial pressure was found to have a greater kinetic impact with the perovskite than with NiO. Conversely, O_2 partial pressure was found to play a lesser role in the kinetics.

4. Discussion

It must be emphasized that the reaction orders listed in Table 3 represent apparent reaction orders and not necessarily true kinetic orders. The distinction arises because of the inherent uncertainties involved with

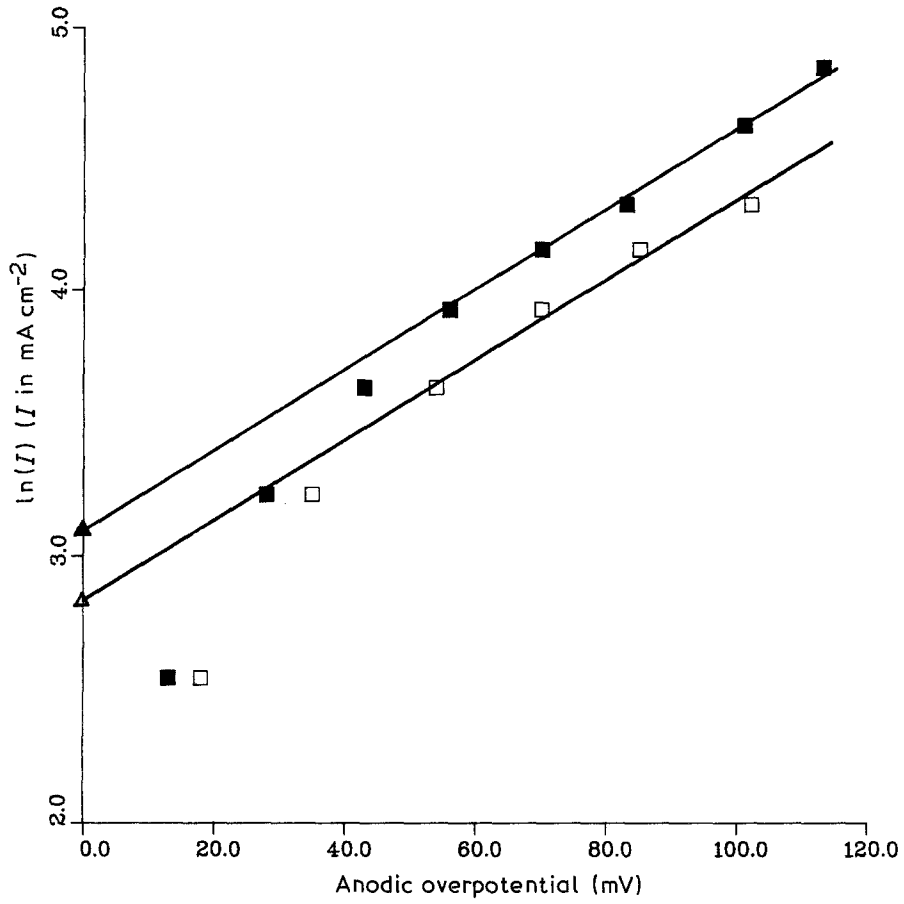

Fig. 10. Tafel plot of anodic polarization data at 590° C. ■ = 50% CO_2, 20% O_2; □ = 10% CO_2, 20% O_2; ▲ = i_0 of the 50/20 oxidant; △ = i_0 of the 10/20 oxidant. Slopes correspond to $\alpha_+ = 1.15$.

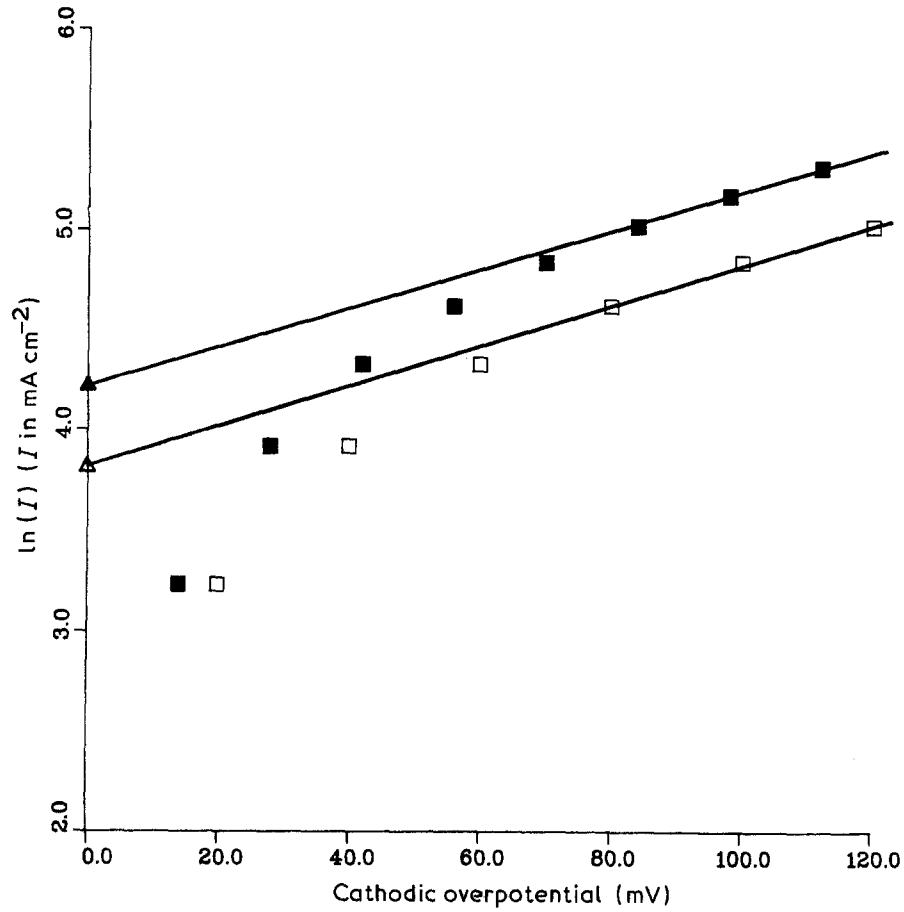

Fig. 11. Tafel plot of cathodic polarization data at 590° C. ■ = 50% CO_2, 20% O_2; □ = 10% CO_2, 20% O_2; ▲ = i_0 of the 50/20 oxidant; △ = i_0 of the 10/20 oxidant. Slopes correspond to $\alpha_- = 0.75$.

Table 3. Calculated reaction orders for CO_2 and O_2 on perovskite and NiO [16] from the polarization data at 590° C from Figs 5, 6, 8, 10 and 11

Condition	*Reaction orders*	
	Perovskite	*NiO*
CO_2, cathodic	+0.70	+0.25
O_2, cathodic	+0.45	+0.65
CO_2, anodic	−0.30	−0.75
O_2, anodic	−0.05	+0.15

porous electrodes. The configuration of the electrode/membrane interface plays a critical role in determining the polarization behavior. Diffusion polarization may become substantial if the active electrode area is not well dispersed or if the electrode surface is not adequately wetted by the carbonate melt. Even under conditions of optimal electrode/membrane contacting, diffusion polarization can introduce significant affects. However, the linear polarization curves we observed, even at very high current densities, suggest electrode/membrane contacting was satisfactory and kinetic control dominated.

A result of primary interest concerns the reaction orders listed in Table 3. Cathodically, CO_2 was found to play a more important role in the kinetics on the perovskite than on NiO. In contrast, O_2 was found to have less kinetic impact on perovskite than on NiO. These results indicate that the optimum CO_2/O_2 ratio for an MCFC oxidant gas stream would be higher for the perovskite than NiO. Thus, the anode exhaust recycle rate to the cathode intake would necessarily be increased with the perovskite.

The reaction orders also indicate there may be a different mechanism on the two materials. The cathodic orders with the perovskite, 0.70 for CO_2 and 0.45 for O_2, are reasonably consistent with the stoichiometry of the overall cathodic reaction

$$CO_2 + \tfrac{1}{2}O_2 + 2e^- \longrightarrow CO_3^{2-} \qquad (11)$$

However, a mechanism which was consistent with both the reaction orders and transfer coefficients could not be determined. This problem has also plagued researchers attempting to decipher the cathodic mechanism on NiO [18].

5. Conclusions

A simple procedure was developed for fabricating porous ceramic electrodes for use in MCFC tests. The technique involves pressing the powdered ceramic, in this case a perovskite-type compound, $La_{0.8}Sr_{0.2}CoO_3$, under relatively low pressure (25 kg cm^{-2}), and then partially sintering the pressed structure at moderate temperature (1100° C). This procedure produced electrode structures of high porosity (65%), good conductivity (~ 1 (ohm cm)$^{-1}$) and reasonable mechanical strength. The MCFC tests indicated the perovskite electrodes were comparable to NiO in mass transfer performance.

The cathodic performance of the perovskite electrodes in an MCFC were compared to that of the standard cathode, NiO. Although the results indicate there may be a different cathodic reaction mechanism on the two materials, the overall kinetic performance of the perovskite was comparable to that of the NiO. The results are encouraging for future use of $La_{0.8}Sr_{0.2}CoO_3$ as the MCFC cathode. However, more extensive research needs to be conducted, with $SrTiO_3$ as the matrix of the electrolyte membrane to assure no long-term stability problems exist.

Acknowledgements

The authors would like to thank the Department of Energy's Pittsburgh Energy Technology Center and Combustion Engineering for financial support. The authors would also like to thank James Smith from the Argonne National Laboratory for helpful suggestions.

References

[1] P. A. Lessing, G. R. Miller and H. Yamada, *J. Electrochem. Soc.* **133** (1986) 1537.
[2] C. D. Iacovangelo and E. C. Jerabek, *J. Electrochem. Soc.* **133** (1986) 280.
[3] J. D. Doyon, T. Gilbert and G. Davies, *J. Electrochem. Soc.* **134** (1987) 3035.
[4] C. E. Baumgartner, *J. Electrochem. Soc.* **131** 8 (1984) 1850.
[5] C. D. Iacovangelo, *J. Electrochem. Soc.* **133** 11 (1986) 2410.
[6] D. A. Shores and P. Singh, in 'Molten Carbonate Fuel Cell Technology' (edited by J. R. Selman and T. D. Claar), The Electrochemical Society Softbound Proceedings Series, Pennington, NJ (1984) p. 271.
[7] E. T. Ong and T. D. Claar, in 'Molten Carbonate Fuel Cell Technology' (edited by J. R. Selman and T. D. Claar), The Electrochemical Society Softbound Proceedings Series, Pennington, NJ (1984) p. 54.
[8] A. Gelb and G. Wilemski, 'Modeling of Long-Term Decay in the Molten Carbonate Fuel Cell', Final Report EPRI-EM-2596, Project 1085-5, September (1982)
[9] H. R. Kunz, *J. Electrochem. Soc.* **134** (1987) 105.
[10] M. D. Ingram and G. J. Janz, *Electrochim. Acta* **10** (1965) 783.
[11] C. E. Baumgartner, R. H. Arendt, C. D. Iacovangelo and B. R. Karas, *J. Electrochem. Soc.* **131** (1984) 2217.
[12] 'Development of Molten Carbonate Fuel Cell Power Plant', Final Report DE/ET/17109-20, Vol. 1 (DE85008743) March (1985) pp. 4–138 to 4–149.
[13] M. D. Franke and J. Winnick, *J. Electrochem. Soc.* **135** (1988) 1595.
[14] Institute of Gas Technology, 'Fuel Cell Research on Second Generation Molten Carbonate Systems', Project 9105 Final Technical Report, April (1979).
[15] Institute of Gas Technology, 'Fuel Cell Research on Second Generation Molten Carbonate Systems', Project 8984 Final Status Report, Sept. (1977).
[16] J. Winnick, and P. N. Ross, *J. Electrochem. Soc.* **128** (1981) 991.
[17] K. J. Vetter, 'Electrochemical Kinetics', Academic Press, New York (1967) pp. 436–438.
[18] H. R. Kunz, L. J. Bregoli and S. T. Szymanski, *J. Electrochem. Soc.* **131** (1984) 2815.